



SPE 46211

Spontaneous Water Imbibition into Diatomite

J. M. Schembre, S. Akin, L. M. Castanier, and A. R. Kovscek. SPE Members, Stanford University

Copyright 1998, Society of Petroleum Engineers, Inc.

This paper was prepared for presentation at the 1998 Western Regional Meeting held in Bakersfield, California, 10-13 May 1998.

This paper was selected for presentation by an SPE Program Committee following review of information contained in an abstract submitted by the author(s). Contents of the paper, as presented, have not been reviewed by the Society of Petroleum Engineers and are subject to correction by the author(s). The material, as presented, does not necessarily reflect any position of the Society of Petroleum Engineers, its officers, or members. Papers presented at SPE meetings are subject to publication review by Editorial Committees of the Society of Petroleum Engineers. Electronic reproduction, distribution, or storage of any part of this paper for commercial purposes without the written consent of the Society of Petroleum Engineers is prohibited. Permission to reproduce in print is restricted to an abstract of not more than 300 words; illustrations may not be copied. The abstract must contain conspicuous acknowledgment of where and by whom the paper was presented. Write Librarian, SPE, P.O. Box 833836, Richardson, TX 75083-3836, U.S.A., fax 01-972-952-9435.

Abstract

A systematic experimental investigation of capillary pressure characteristics and fluid flow in diatomite has been accomplished. Using an X-ray CT scanner and a specially constructed imbibition cell, we study spontaneous water imbibition processes in diatomite and for reference Berea sandstone and chalk. The mass of water imbibed as a function of time is also measured. Imbibition is restricted to cocurrent flow. Despite a marked difference in rock properties including permeability and porosity, we find similar trends in saturation profiles and weight gain versus time functions. Imbibition in diatomite is relatively rapid when initial water saturation is low due to large capillary forces.

Introduction

Water imbibition is fundamental to both waterflood and steamdrive performance in low permeability reservoir rocks such as diatomite and chalk. Imbibition is an immiscible displacement process, whereby a non-wetting fluid within a porous medium is spontaneously expelled by wetting fluid that surrounds the medium and is drawn into the medium by capillary suction. This phenomenon is caused by the differential attraction forces between the pore walls and fluids. The rate of imbibition is primarily dependent on the rock permeability, pore structure, wettability, and the interfacial tension between the resident phase and the imbibing phase. On the macroscopic scale, capillary imbibition forces determine, in part, how rapidly and easily a hydraulically fractured water injector injects water into a low permeability formation and at what rate the injected water

propagates. In naturally fractured systems with a high degree of interconnectedness, imbibition forces must be strong for a waterflood to be successful. If they are not, water will propagate through the fracture network from injector to producer and the waterflood will fail.

Capillary phenomena are equally important during steam injection into diatomite or lower permeability sandstones. Steam injection, especially at short times, is accompanied by condensation and flow of the resulting hot water away from the injector. Likewise, for live steam to enter the matrix of a low permeability rock, a substantial capillary entry pressure must be overcome. Producers might also suffer from capillary effects as the formation attempts to maintain capillary equilibrium with fluids in the production hydraulic fracture and the well.

Because of the importance of imbibition on oil recovery, it has been studied widely. However, our knowledge of hydrocarbon recovery and fluid displacement in porous media is less than complete. To date, much of the focus on imbibition has centered on carbonaceous rocks. This is a result of the importance of the North Sea Chalks¹, the West Texas Carbonates, and the Middle Eastern Limestones.

Before describing the experimental apparatus, procedures, and results, we briefly review some theory regarding imbibition. This review helps to put experimental results into context and will simplify the discussion to follow.

Imbibition. Handy² provides a classic analysis and experimental investigation of the dynamics of imbibition in sandstone. He examines imbibition in the limit that capillary forces dominate over buoyancy and viscous forces, and displacement occurs vertically upward. Mainly, air-water systems are examined. It is noted that imbibition could be described by either a diffusion-like equation or a frontal-advance equation, depending on assumptions. In the former, the diffusion coefficient is proportional to the partial derivative of capillary pressure with respect to water saturation and computed displacement fronts are significantly diffuse. Whereas in the latter, the velocity of the imbibed phase is proportional to the gradient of capillary pressure with respect to distance, and fronts are assumed to be sharp. The main difference between the two descriptions is that the diffusion equation predicts that the smallest pores fill first

and the larger pores fill later. The frontal advance equation assumes that pores of all sizes fill simultaneously because large pores are connected to small pores, and *vice versa*. Thus, it is hard to fill the small pores selectively.

Both developments predict that the mass of water imbibed is a linear function of the square root of time and experiments agree with this dependence. However, the end of imbibition is quite abrupt which is contrary to the expected result for a diffusive-type process. This observation lead Handy to assert that the frontal advance equation more nearly described the true process. Indeed, recent experiments where the position and shape of a water imbibition front in a homogeneous Berea sandstone were accurately tracked indicate relatively sharp and steep fronts³. These experiments were also modeled numerically with a diffusion equation incorporating buoyancy driven advection. The authors note that the computed saturation profiles are not sufficiently sharp at the displacement front to match the experimentally determined profiles. Also, water breakthrough occurs too early in the calculations.

Upon assuming that water imbibes in a piston-like manner, gas viscosity is negligible, capillary forces outweigh gravity forces, and the spatial gradient of capillary pressure is linear, the mass of imbibed water is given by

$$m = \rho_w A \left(\frac{2P_c k \phi S_w}{\mu_w} \right)^{1/2} t^{1/2} \quad (1)$$

In Eq. (1), m is the mass of water imbibed, ρ_w is the density of water, A is the cross-sectional area, P_c is the capillary pressure, k is the permeability to water, ϕ is the porosity, S_w the aqueous phase saturation, μ_w is the viscosity, and t is the time. The linear relation between the mass imbibed and the square root of time is apparent and the slope is proportional to the square root of the product of $P_c k S_w$. Dimensional analysis teaches that this quantity has units of force and it is a measure of the likelihood of imbibition. Intuitively, it is expected that the larger is $P_c k S_w$, the more rapidly a porous medium imbibes spontaneously. For simplicity, we refer to $P_c k S_w$ as the imbibition potential.

Spontaneous imbibition is perhaps the most important phenomenon in oil recovery from fractured reservoirs. For such reservoirs, the rate of mass transfer between the rock matrix and fractures usually determines the oil production⁴. Imbibition is also essential in evaluation of the rock wettability^{5,6}. For spontaneous imbibition, the main driving force is capillary suction. Because of strong capillary forces, the smallest pore bodies that are next to the interface are always invaded first. Usually, the displacement takes place at small but finite capillary numbers⁷. The rate of imbibition is usually a function of porous media and fluid properties such as absolute and relative permeability, viscosity, interfacial tension, and wettability⁸. Most experimental work on imbibition behavior has concentrated on the scaling aspects of the process in order estimate oil recovery from reservoir

matrix blocks that have shapes, and sizes different from those of the laboratory core samples⁵.

Kazemi et al.⁹ presented numerical and analytical solutions of oil recovery using empirical, exponential transfer functions based on the data given by Aronofsky et al.¹⁰ and Mattax and Kyte¹¹. They proposed a shape factor which included the effect of size, shape, and boundary conditions of the matrix. More recently, this shape factor was generalized by Ma et al.¹² to account for the effect of viscosity ratio, sample shape, and boundary conditions. They proposed a dimensionless time, t_D , equation based on the porosity, ϕ , absolute permeability, k , interfacial tension, σ , and a characteristic length, L_c , as shown below:

$$t_D = t \sqrt{\frac{k}{\phi} \frac{\sigma}{\mu_s L_c^2}} \quad (2)$$

The geometric average of viscosities and the characteristic length is given by the following equations:

$$\mu_s = \sqrt{\mu_w \mu_{mw}} \quad (3)$$

$$L_c = \sqrt{\frac{V_b}{\sum_{i=1}^n \frac{A_i}{l_{Ai}}} } \quad (4)$$

where V_b is the bulk volume, A_i is the area open to imbibition at the i^{th} direction, and l_{Ai} is the distance traveled by the imbibition front from the open surface to the no-flow boundary. The above scaling equation was used by Zhang et al.⁸ and they reported that ultimate oil recovery on a pore volume basis by spontaneous imbibition in Berea sandstone cores is approximately constant for systems with differing lengths, viscosity ratios, and boundary conditions.

Diatomite. An important class of low permeability rock that remains relatively unstudied is diatomite. Diatomite is a hydrous form of silica or opal composed of the remains of microscopic shells of diatoms, which are single-celled aquatic plankton¹³. Diatomites are very porous (frequently exceeding 50%) with high internal surface area, but they are exceptionally impermeable¹⁴. Permeabilities range from 0.1 to 10 mD. Diatomite is commercially important¹⁵. Estimates of the original oil in place for the California diatomites (Kern Co., CA) range from 10 to 15 billion barrels¹⁶. Reservoir rock is assumed to be strongly to moderately water wet. Because the formations are very porous and the initial oil saturation is large (35 to 70%), the target for potential production is high¹⁷.

Multiphase flow in diatomite is dominated by capillary forces. Yet, a detailed scan of the literature shows few reported capillary pressure curves and little information on the extent and rate of imbibition¹⁷. Likewise, the mechanisms

of oil displacement and trapping are unclear, but presumed to be similar to those in sandstone. However, rock morphology is very different¹⁸.

Thus, it seems helpful to undertake a systematic study of fluid transport in diatomite; it appears that capillary driven flow is relevant to reservoir flow processes. In this work, our main focus is the design of a CT monitorable experimental apparatus and the study of one-dimensional spontaneous imbibition of water into air-filled diatomite. This simpler system provides some understanding of the behavior of water-oil-rock systems³. Work on the oil-water system is underway¹⁹. For contrast, we conduct experiments with a typical sandstone and chalk. Thus, we illustrate the effects of pore structure, permeability, and porosity on imbibition. The progress and effectiveness of imbibition fronts is monitored using an X-ray CT scanner and a specially constructed imbibition cell.

Experimental Details

The rock samples used in this study were Berea sandstone, diatomite, and chalk. Their description is given in Table 1. The Berea cores were both cylindrical and square shaped (core 1 and core 2, respectively). The diatomite (core 3), an outcrop from Lompoc, California, and chalk (core 4), an outcrop from Kansas (core 4) were cylindrical shaped (Table 1). The objective of using differently shaped, but similar cross-sectional area, Berea sandstone cores was to confirm that cross-sectional shape did not influence results.

The Berea and chalk were cored using conventional drilling and cutting methods. In the case of the diatomite, the core could not be formed by the same method due to its fragile structure. Thus, a piece of the rock is cut by band saw to approximate dimensions, and it is shaped manually by fixing two circular 1 inch-diameter patterns, held at both ends of the rock. These pieces are used as guides in the shaping process with a file. Final shaping is achieved with sandpaper.

The sandstone samples are fired at 450 °C for 12 hours to remove the effect of clay swelling and migration during the imbibition process. Diatomite and chalk are not fired. The cores are then sealed with epoxy on the sides parallel to the flow direction to obtain one-dimensional imbibition (See Fig. 1). It is important to mention that, in the case of the diatomite, the coating is a very critical process since the epoxy does not adhere securely to the surface. Without care, de-lamination of the epoxy coat occurs after some use of the sample.

Our objective is to obtain the change of average water saturation with time, the time rate of imbibition, and to calculate the imbibition potential term from the slope of the average water saturation versus the square root of time. Thus far, we have concentrated on water imbibition into air-filled cores. Water-oil experiments have been conducted also¹⁹.

The weight gain of the core was measured by two methods. Initially, the sample core was suspended by means

of an acrylic and steel frame directly from a weighing balance in an acrylic container filled with water. Although this method gives good results, we found some disadvantages in the handling of the core when CT-imaging was performed. Mainly, asymmetry in the scanning plane leads to unavoidable X-shaped beam hardening artifacts. The design of an imbibition cell that permitted CT-scanning of the core during the imbibition process and minimized artifacts was necessary.

Description of Experimental Cell. The experimental cell, shown schematically in Fig. 1, is constructed from acrylic tubes, and it consists of two separate chambers. The main chamber is the core holder, and it is surrounded by the second chamber that is filled with water to reduce possible beam hardening. Beam hardening refers to the differential adsorption of longer wavelength X-rays and leads to shadows around the periphery of CT images. There is no fluid exchange between containers and the outer water-filled chamber allows for some measure of temperature control. The core holder has two end caps for fluids to flow in and out of the core holder. The inlet cap at the bottom of the core holder is connected to a fluid tank through a rubber tube. The weight of imbibed fluid is measured directly by means of a balance as shown in Fig. 2. Displaced fluids exit from the top.

The CT-Scanner used is a Picker™ 1200 SX X-ray scanner with 1200 fixed detectors. The voxel dimension is (0.5 mm by 0.5 mm by 5 mm), the tube current is 65 mA, and the energy level of the radiation is 140 keV. The porosity and aqueous-phase saturation fields are measured on a single vertical volume section in the center of the core as a function of time. The acquisition time of one image is 3 seconds while the processing time is around 40 seconds. The total time of measurement is short enough to capture accurately the position of the front and construct the saturation profiles along the core.

Experimental Procedure. After preparation and coating, the core is exposed to house vacuum and a temperature of 50 °C, for 10 hours. This ensures a “dry” core at the beginning of the experiment. The procedure is as follows:

1. The dry core is placed in the core holder (main chamber).
2. A paper filter is placed at the bottom of the core. The objective is to obtain a uniform distribution of water at the bottom rock face.
3. Since the core holder is surrounded by water during the CT-experiments, a leak test is performed by applying a slight gas pressure and checking that the pressure in the core holder is maintained for a period of time.
4. The core holder is placed in the second chamber and leveled.

In the cases where CT scanning is performed, the water jacket is filled with water. Water is introduced to the open

bottom face of the core and the progress of the imbibition front monitored with frequent CT-scans.

Since imbibition is spontaneous, care was taken to maintain the water level in the core holder so that it just contacts the rock base. The data acquisition system for the balance is started. Once the imbibition begins, the weight of the water reservoir is recorded every 10 seconds. The gain of weight in the core is computed directly by the change of weight measured in the tank containing the water. The reference weight corresponds to time equal to zero in which tubing is filled with water and the water-air interface is just below the bottom face of the core.

In the case where CT-Scanning is performed, dry images of the core are taken to obtain the reference dry core CT-values. Scanning is performed every 50 seconds for the first 5 minutes. Afterwards the intervals between the images are longer since the change of saturation in the core becomes slower with time.

The data acquisition process is stopped when changes in the weight are no longer observed. Also, constant water saturation is verified by measuring the average CT-number and standard deviation in the image of the core and verifying that it is the same from one scan to another. In order to have a reference wet image of the core, a final scan is conducted at least 12 hours later. After spontaneous imbibition is complete, degassed water is pumped through the core to ensure 100% water saturation.

Data Processing. Once the weight-gain data is collected during the spontaneous imbibition process, it is converted into weight imbibed into the core and a linear regression is performed to obtain the slope of the resulting straight line. This correlates the weight gain of the core to the square root of time.

For CT-number related calculations, the map of porosity and the saturation profiles are obtained using the method of subtraction of images of raw CT data²⁰. Thus, in the case of the porosity

$$\phi = \frac{CT_{wet} - CT_{dry}}{CT_{water} - CT_{air}} \quad (5)$$

where,

CT_{wet} : CT value for a fully water saturated core, obtained from a last scan performed after 12 hours or more of water imbibition.

CT_{dry} : CT value for the dry core, obtained from the scanning of the core before the imbibition process starts

CT_{water} : CT value of water

CT_{air} : CT value of air

It is important to note that CT_{wet} corresponds to 100% water saturation. This is verified by comparing the porosity fields computed from the dry and water-filled images. When

the core is completely saturated, they are the same.

To construct saturation profiles we use

$$S_w = \frac{CT_{obj} - CT_{dry}}{CT_{wet} - CT_{dry}} \quad (6)$$

where CT_{obj} is the CT value of the image being processed.

Results

First, we present and summarize weight gain as a function of time and then the corresponding CT-images of the imbibition process are given.

Weight Gain Plots. Data obtained from the imbibition experiments for the different cores were converted into the weight of water imbibed as a function of time in order to measure the rate of change of water saturation in the core. The results are summarized in Table 2.

Figure 3 shows plots of the dimensionless weight gain versus the dimensionless square root of time for the Berea sandstone imbibition experiment obtained by utilizing Eq. (2). Three different sets of symbols indicate three different experiments. In this case, the weight gain was measured directly by hanging the core from a balance and bringing a beaker of water up until it just touched the bottom of the core, as described in the experimental section. Discrepancy in the early time response is explained by the level of the free water surface in contact with the bottom of the core. Because the core is slightly submerged, imbibition is forced and the response is faster than expected. Once the water front passes the free water level, this effect ceases. Note that all experimental runs show a good reproducibility. Spontaneous imbibition ends when the water front reaches the end of the core. This time is practically the same for all three cases.

Next, a series of experiments were performed in Berea sandstone cores to confirm that the cross-sectional shape of the cores did not bias our results. Cores with both circular and square cross-sectional areas, as shown in Fig. 4, were used. The straight-line portion in both cases has a similar slope. The initial difference in the total weight gain is probably due to the fact that the core with square cross-sectional area did not imbibe immediately because, initially, the end of the core was not fully submerged in water. However, these results convinced us to use cylindrical diatomite cores despite the difficulties associated with manual shaping.

These initial experiments with Berea sandstone confirmed that our experimental approach was adequate to collect the data required. Imbibition in diatomite was considered next. Figure 5 shows weight gain obtained for the diatomite during two different experiments. All diatomite experiments were conducted in the imbibition cell. Again, there is some deviation from linearity in the initial stages of imbibition. For later times, the response is similar. This deviation can be explained by reasons related to the experimental method.

Experiments conducted in the imbibition cell also have the possibility that the water level of the tank is not exactly equal to that of the bottom of the core. Forced imbibition could exist for a short time. The second explanation is the filter paper at the bottom of the imbibition cell, which might not saturate uniformly at the beginning of the imbibition process. Thus, imbibition is retarded. Interestingly, the water imbibition process is quite rapid despite the low permeability of diatomite. These diatomite samples imbibe water at rates rivaling sandstone.

For comparison, experiments on a low permeability chalk sample were also conducted. Figure 6 shows the results. The trend of weight gain is not as smooth as either the sandstone or diatomite case. But, we do observe, overall, a relatively similar trend. Heterogeneities observed during CT-scanning account for the jaggedness of the weight gain. These heterogeneities will be discussed further in the next section. Spontaneous imbibition in the chalk is much slower than in either the Berea sandstone or diatomite, as indicated by the length of time necessary to complete imbibition.

To further the analysis, and quantify the degree of spontaneous imbibition, a linear regression was performed on the straight line portions of dimensionless weight gain versus square root of dimensionless time plots to obtain the slope. Table 2 shows (a) the slope, (b) the porosity of the samples obtained by Eq. (5), (c) the imbibition potential calculated by Eq. (1) and, (d) the slope divided by the cross-sectional area for each experiment. In the case of Berea sandstone with circular cross-sectional area, the three different experiments show similar slope, confirming the repeatability of the method. Also, a similar slope is found for the experiment on square cross-sectional area cores.

The diatomite shows the highest values for slope and imbibition potential. The average imbibition potential for diatomite is 0.0060 dyne, whereas it is only 0.0045 dyne for the sandstone and 0.0038 dyne for the chalk. We find that capillary forces during the spontaneous imbibition process make a contribution to flow that offsets the low permeability of the diatomite.

A recovery model proposed by Gupta and Civan²¹ is used to interpret the imbibition experiments conducted using the aforementioned rocks. This triple exponent, recovery model considers an imbibition process in which wetting phase displaces the nonwetting phase honoring transfer of the nonwetting phase from the dead-end pores to the network of interconnected pores (a_3 and λ_{3D}) from the network to the matrix-fracture interface (a_1 and λ_{1D}), and finally from the interface to the fracture system (a_2 and λ_{2D}). The summation of the coefficients, a_i is 1. The dimensionless form of this model is given by the following equation:

$$w_D = 1 - a_1 e^{-\lambda_{1D} t_D} - a_2 e^{-\lambda_{2D} t_D} - a_3 e^{-\lambda_{3D} t_D} \quad (7)$$

where the dimensionless rate constants, λ_{iD} , are defined as

$$\lambda_{iD} = \frac{\lambda_i}{\left[\frac{\sigma \cos(\theta) F_s}{\mu_w} \sqrt{\frac{k}{\phi}} \right]} \quad (8)$$

The coefficients a_i , and λ_{iD} are determined numerically by minimizing the observed dimensionless weight gain data and the one given by Eq. (7) using a genetic algorithm²². Figure 6 presents the experimental data scaled by using the dimensionless time given in Eq. (2) as well as the model curves for Berea sandstone, diatomite, and chalk. Good agreement between model and experimental data was observed for both cases apart from slight deviations at early time intervals. The aforementioned initial nonlinear flow period is probably responsible from this mismatch. For both rock types it was observed that the contact angle is zero, indicating a water-wet system (Table 3). For chalk, it was observed that the main dimensionless imbibition parameter λ_{1D} was high and λ_{2D} , and λ_{3D} were identical. This is in agreement with Gupta and Civan's findings for chalk imbibition data presented by Cuiec et al¹. For Berea sandstone and chalk, the optimized value for λ_{1D} is smaller compared to diatomite. This implies that the spontaneous imbibition is more effective in diatomite than sandstone and chalk. We also found that the contribution of dead-end pores to the imbibition process in sandstone and chalk is small (λ_{3D} is small) indicating that the amount of recoverable non-wetting phase in the dead-end pore space is insignificant. However, for diatomite, a_3 was found to be zero. This suggests that during spontaneous imbibition in diatomites, pores of all sizes fill simultaneously which implies that large pores are interconnected to small pores. This observation is consistent with the complex, small-diameter pore network of diatomites²³. Thus, it is hard to fill the very small pores selectively, leaving relatively large pores unfilled. CT derived water saturation images support this theory as explained in the following section.

CT-Scanning Results. Porosity maps and the water saturation profiles obtained during the imbibition for the Berea sandstone, diatomite and chalk are shown in Figs 7, 8, and 9, respectively. Porosity images are obtained using Eq. (5) and saturation images using Eq. (6). Both water saturation and porosity are indicated by gray-scale shading. In the case of water saturation images, black indicates no water and white indicates fully water saturated. Porosity maps are located in the right-hand corner. The shading scale for the porosity images is compressed to highlight heterogeneity, but again black is small and white is large.

Sandstone porosity ranges from 0.08 to 0.23. The Berea sandstone images in Fig. 7 show some surprising results. The weight gain data agree with a piston-like assumption, but images of the water displacement front are not truly piston like. Initially, water enters at the center of the core.

Intuitively, we expect capillary forces to spread the saturation front laterally as well as upward. However, the front is slightly rounded and centered in the middle of the core (refer to Fig. 7 at 240 s). The leading edge of the water front moves through the core maintaining its rounded shape until reaching the core outlet. At about 60 s, the water saturation front does span the cross-section of the core at the inlet. This rear portion of the water front appears to move through the core displacing any remaining gas. Interestingly, the time taken for the rounded water saturation front to span the core (60 s) corresponds roughly with the onset of linear weight gain in Fig. 7 ($10 \text{ s}^{1/2}$).

The porosity map for diatomite shown in Fig. 8 indicates that this sample is relatively homogeneous and average porosity is about 65%. Strong capillary forces are evident in the CT images for imbibition in diatomite. Water again enters the core in the center, but it spreads laterally quite rapidly. The water front is sharp and the displacement is clearly piston like. As the front progresses down the core it diffuses somewhat. The water front reaches the end of the core in about 3600 s. The CT images correspond to the lower curve in Fig. 5 that deviated from linearity at short time. Figure 8 shows that the saturation front was not piston like until roughly 90 s. Hence, the deviation from linearity results from the non-uniform displacement front.

In contrast to the sandstone and diatomite samples, the chalk core contains some heterogeneities. These are evident in the porosity map as given in Fig. 9. For instance, there is a dark portion, indicating low porosity, on the left hand side about a quarter of the way up the chalk core. Chalk porosity ranges from 0.15 to 0.25. Like the diatomite, the chalk shows a practically uniform and sharp front at the beginning that becomes less sharp at later times. It is interesting to note that the heterogeneities fill with water at somewhat different rates. The slow filling of the above mentioned heterogeneity is evident in the saturation images at 300, 540, and 600 s.

A comparison of the time necessary for spontaneous imbibition to be completed in each type of rock, confirms the weight gain results. Diatomite takes about three times longer than Berea sandstone, while the chalk takes ten to eleven times. It is important to recall that the pore volume of the diatomite is about five times the pore volume of the Berea sandstone.

Discussion

The simple water displacing air experiments provide some insight into the capillary pressure characteristics of diatomite. Denote the imbibition potential by IP and take the ratio of diatomite IP to sandstone:

$$\frac{IP_d}{IP_s} = \frac{(P_c k S_w)_d}{(P_c k S_w)_s} \quad (9)$$

where the subscripts d and s refer to diatomite and sandstone, respectively. Using average values from Table 3, this

quantity is 2.4 indicating the strong tendency of diatomite to imbibe water. From Figs. 7 and 8, we judge that the water saturation upstream of the saturation front is about 1. So, the ratio of saturations in Eq. (9) is about 1. Next, we replace P_c with the appropriate Leverett J-function²⁴:

$$P_c = \sigma \left(\frac{\phi}{k} \right)^{1/2} J(S_w) \quad (10)$$

for water wet rocks. In Eq. (10), σ is the air-water interfacial tension and $J(S_w)$ is the Leverett J-function. Upon some rearrangement

$$\frac{IP_d}{IP_s} = \left(\frac{k_d}{k_s} \right)^{1/2} \left(\frac{\phi_d}{\phi_s} \right)^{1/2} \left(\frac{J_d(S_w)}{J_s(S_w)} \right) > 1 \quad (11)$$

Equation (11) teaches us about the magnitude of the J-function for diatomite. The first term in parentheses on the right is clearly less than 1 because diatomite is less permeable than sandstone. With typical sandstone (100 to 1000 md) and diatomite (0.1 to 10 md) permeabilities, k_d/k_s might range from 0.1 to 10^{-4} . Table 3 shows that the diatomite samples are roughly 4 times as porous as the sandstone. For Eq. (11) to be greater than 1, J_d/J_s must be greater than 1. This explains, in part, why the relatively impermeable diatomite imbibes strongly when the rock is initially filled with air. Likewise, it explains why diatomite recoveries lie to the left of the sandstone and chalk in Fig. 6.

Another interesting aspect of these experiments is the very low trapped gas saturation. For instance, Fig. 8 at 4800 s shows water saturation in excess of 95% shortly after breakthrough. The strong capillary forces and the small pore throat to body aspect ratio of diatomite suggests much snap-off and trapped gas. However, for snap-off to occur, pore corners and crevices must fill with wetting liquid and sufficient liquid for snap-off must accumulate at pore throats before the pore is filled completely by the advancing imbibition front. We speculate that trapped gas saturation is low because the advancing front fills pores with water at least as rapidly as pore corners fill with water. Indeed, recent pore-level network modeling of imbibition shows that in the absence of flow in pore corners the displacement pattern is a flat front with little or no trapping of the nonwetting phase²⁵.

Conclusions

An experimental apparatus and method to permit the collection of data and CT images during spontaneous imbibition was designed. The samples examined were Berea sandstone, diatomite and chalk, which allowed the study and comparison of the contribution of porosity, permeability, and capillary forces during imbibition. Several tests were performed and they confirmed the repeatability of the method. The water/air system was examined extensively. It was confirmed that different core cross-sectional areas did not bias results.

CT imaging of the imbibition process permitted not only

the observation of the advance of the water front into the cores but explains the observed trends in weight gain as a function of time. Images obtained for diatomites and chalk show a homogeneous and piston-like water front during the process. Results for sandstone showed good agreement with previous work^{2,3,26} and permitted the comparison of imbibition potential for different types of rocks. In impermeable diatomite, capillary forces result in a strong imbibition potential for water.

Future Work

The results obtained here are encouraging. We have turned our attention to the oil-water system. In addition to conducting spontaneous imbibition experiments, we are developing a matching procedure to extract capillary pressure and relative permeability data.

Nomenclature

a_i	= constant, dimensionless
A	= cross-sectional area, L^2
CT_{wet}	= CT value for a fully water saturated core
CT_{dry}	= CT value for the dry core
CT_{water}	= CT value of water
CT_{air}	= CT value of air
CT_{obj}	= CT value of the image being processed
F_s	= shape factor, dimensionless
IP	= imbibition potential, LMT^2
$J(S_w)$	= Leverett J-function, dimensionless
k	= permeability, L^2
L_c	= critical length, L
λ	= rate constant, dimensionless
m	= mass of water imbibed, M
ρ_w	= water density, mL^{-3}
S	= area, L^2
S_w	= water saturation, dimensionless
P_c	= capillary pressure, $ML^{-1}T^{-2}$
t	= time, T
ϕ	= porosity, dimensionless
σ	= interfacial tension, MT^{-2}
μ_w	= water viscosity, $ML^{-1}T^{-1}$
V	= volume, L^3
w_d	= weight gain, dimensionless

Subscripts

b	= bulk
d	= diatomite or dimensionless
s	= sandstone

SI Metric Conversion Factors

dyne x 1.000 000	E-05 = newton (N)
md x 6.894 757	E+00 = μm^2
Celsius x kelvin (K)	$T_K = T_{C+} + 273.15$

Acknowledgments

This work was supported by the Assistant Secretary for Fossil Energy, Office of Oil, Gas and Shale Technologies of the U.S. Department of Energy, under contract No. DE-FG22-96BC14994 to Stanford University. The support of the SUPRI-A Industrial Affiliates is likewise gratefully acknowledged.

References

1. Cuiec L., Bourbiaux B., and Kalaydjian F.: "Oil Recovery by Imbibition in Low-Permeability Chalk," SPE Formation Evaluation Sept. 1994, 200-208.
2. Handy, L.L.: "Determination of Effective Capillary Pressures for Porous Media from Imbibition Data," *Petroleum Transactions, AIME*, **219**(1960) 75-80.
3. Garg, A., E. Zwahlen, and T.W. Patzek: "Experimental and Numerical Studies of One-Dimensional Imbibition in Berea Sandstone," Proceedings of the The Sixteenth Annual American Geophysical Union Hydrology Days, Fort Collins, CO (April 15-18, 1996).
4. Warren J.E., and Root P.J.: "The Behavior of Naturally Fractured Reservoirs," SPE Journal, 245-255, Sept. 1963.
5. Morrow N.R., Ma S., Zhou X., and Zhang X.: "Characterization of Wettability from Spontaneous Imbibition Measurements," paper CIM 94-475, presented at the 45th Annual Technical Meeting of the Petroleum Society of the CIM held in Calgary, Canada, June 12-15, 1994.
6. Jadhunandan P.P, and Morrow, N.R.: "Spontaneous Imbibition of Water by Crude Oil/Brine/Rock Systems," In Situ, Vol. 15. No 4, 319-345, (1991).
7. Sahimi M. *Flow and Transport in Porous Media and Fractured Rock: From Classical Methods to Modern Approaches*, VCH Verlagsgesellschaft mbH, Weinheim, Germany, 1995, 482 pp.
8. Zhang X., Morrow N.R., and Ma S.: "Experimental Verification of a Modified Scaling Group for Spontaneous Imbibition," SPE Reservoir Engineering, Nov. 1996, 280-285.
9. Kazemi H., Gilman J.R., and El-Sharkaway A.M.: "Analytical and Numerical Solution of Oil Recovery From Fractured Reservoirs Using Empirical Transfer Functions," paper SPE 19849, proceedings of the SPE 64th Annual Technical Conference and Exhibition held in San Antonio, TX, Oct. 8-11, 1989, 827-842.
10. Aranofsky J.S, Masse L., and Natanson S.G.: "A Model for the Mechanism of Oil Recovery from the Porous Matrix Due to Water Invasion in Fractured Reservoirs," Trans. AIME, 213, pp 17, 1958.
11. Mattax C.C., and KYTE J.R.: "Imbibition Oil Recovery From Fractured, Water-Drive Reservoirs," SPE Journal 177-184, June 1962, Trans. AIME, 225.
12. Ma S., Zhang X., and Morrow N.R.: "A Characteristic Length for Scaling of Mass Transfer Between Fractures and Matrix," paper SPE 30232 available from SPE, Richardson, 1995.
13. Stosur, J.J. and A. David: "Petrophysical Evaluation of the Diatomite Formation of the Lost Hills Field, California," *Jour. of Petroleum Tech.*, **28**(October) (1971) 1138-1144.
14. Schwartz, D.E.: "Characterizing the Lithology, Petrophysical Properties, and Depositional Setting of the Belridge Diatomite, South Belridge Field, Kern County, California", in *Studies of the Geology of the San Joaquin Basin*, S.A.Graham and H.C.

Olson, Editors, Society of Economic Paleontologists and Mineralogists, Los Angeles, (1988) p. 281-302.

15. "Shell Expanding Belridge Diatomite Program," *Oil and Gas Journal*, **92**(April 11) (1994) 40-42.
16. Ilderton, D.C., T.W. Patzek, J.W. Rector, and H.J. Vinegar: "Passive Imaging of Hydrofractures in the South Belridge Diatomite," *SPE Formation Evaluation*, **March** (1996) 46-54.
17. Wendel D. J., Kunkel L. A., and Swanson G. S.: "Waterflood Potential of Diatomite: New Laboratory Methods," paper SPE 17439 proceedings of the 1988 Western Regional Meeting held in Long Beach, California, 373-81, (23-25 March 1988).
18. Bhat, S.K., and A.R. Kovsky: "Modeling Permeability Alteration in Diatomite Reservoirs During Steam Drive," SUPRI TR 113 Report prepared for US DOE under contract No. DE-FG22-96BC14994 to Stanford University, July 1998.
19. Akin S., and Kovsky A.R.: "Oil Recovery by Imbibition in Low Permeability Diatomite," paper submitted to SPE Western Regional Meeting to be held in Anchorage, Alaska, 1999.
20. Garg, A., A.R. Kovsky, M. Nikrakesh, L.M. Castanier, and T.W. Patzek: "CT Scan and Neural Network Technology for Construction of Detailed Distribution of Residual Oil Saturation During Waterflooding," SPE 35737, in Proceedings of the Western Regional Meeting, Anchorage, Alaska (May 22-24, 1996).
21. Gupta A., and Civan F.: "An Improved Model for Laboratory Measurement of Matrix to Fracture Transfer Function Parameters in Immiscible Displacement," paper SPE 28929 proceedings of the SPE 69th Annual Technical Conference and Exhibition held in New Orleans, LA, USA, 25-28 Sept. 1994.
22. Akin, S., and Demiral, B. : "Genetic Algorithm for Estimating Relative Permeabilities from Displacement Experiments" *Computers and Geosciences*, Vol. 24, No 3, pp. 251-258, (1998).
23. Fassihi M.R., Abu-Khamsin S., Brigham W.E., Williams L.A., and Graham S.A.: "A Preliminary Study of In-Situ Combustion in Diatomites," paper SPE 10701 proceedings of the 1982 SPE California Regional Meeting, San Francisco, March 24-26, 1982, pp. 391-408.
24. Leverett, M.C.: "Capillary Behavior in Porous Solids," *Trans., AIME*, **142**(1941) 152-169.
25. Blunt, M.J. and H. Scher: "Pore-Level Modeling of Wetting," *Physical Review E: Statistical Physics, Plasmas, Fluids, and Related Interdisciplinary Topics*, **52**(6) (1995) 6387-6403.
26. Babadagli, T. and I. Ershaghi: "Imbibition Assisted Two-Phase Flow in Natural Fractures," SPE 24044, in Proceedings of the Western Regional Meeting of the Society of Petroleum Engineers, Bakersfield, CA (March 30 - April 1, 1992).

Table 2: Results obtained for spontaneous imbibition in different experiments.

Core	Rock Type	Slope gr/sec ^{0.5} (1E1)	ϕ %	Imbibition Potential dyne (1E3)	Slope/A gr/sec ^{0.5} / cm ² (1E2)
1	Berea	1.4226	15	3.9953	3.462
1	Berea	1.4883	15	4.4479	3.665
1	Berea	1.499	15	5.1705	3.938
2	Berea	1.4723	15	4.3357	3.607
3	Diatomite	4.4803	65	5.9118	8.771
3	Diatomite	4.331	65	6.1461	8.939
4	Chalk	0.6051	21	0.3845	1.271

Table 3: Interpretations for imbibition experiments.

	a_1	a_2	a_3	λ_{1D}	λ_{2D}	λ_{3D}	θ
Diatomite	0.13	0.87	0.00	5.002	0.0897	0.0	0
Chalk	0.17	0.78	0.05	0.207	0.0042	0.0042	0
Berea	0.1	0.09	0.81	0.179	0.0000	0.0142	0

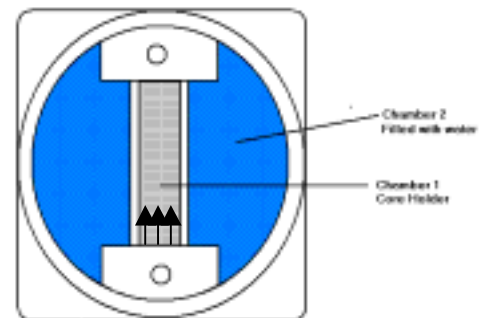


Figure 1. Side view of the imbibition cell showing the two chambers.

Table 1: Rock sample characteristics

Core	Rock Type	Shape	Length cm	D cm	ϕ %
1	Berea	O	11.0	2	15
2	Berea	□	9.0	1.7	15
3	Diatomite	O	8.43	2.5	65
4	Chalk	O	10.0	2.5	21

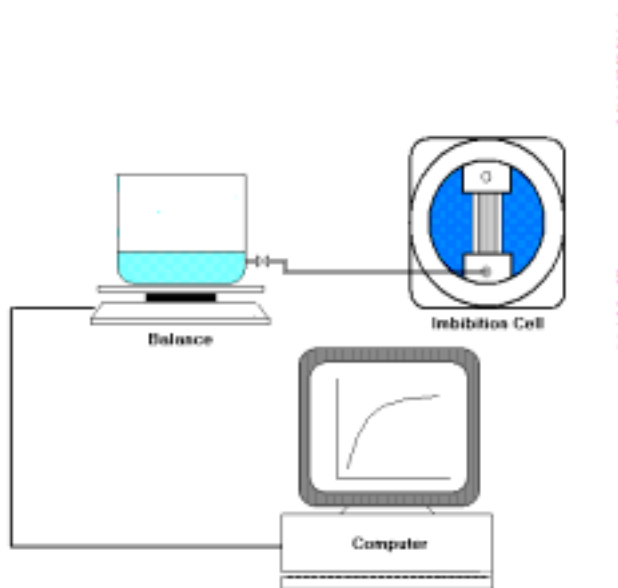


Figure 2. Schematic representation of experimental setup for CT scanning and recording of the change in the weight of the core.

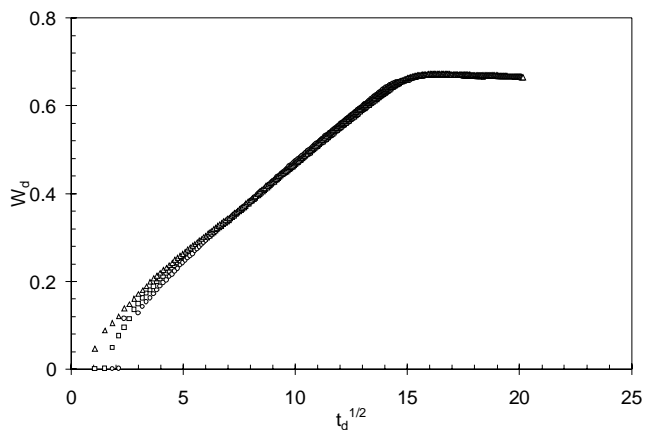


Figure 3. Spontaneous imbibition in Berea sandstone repeatability tests.

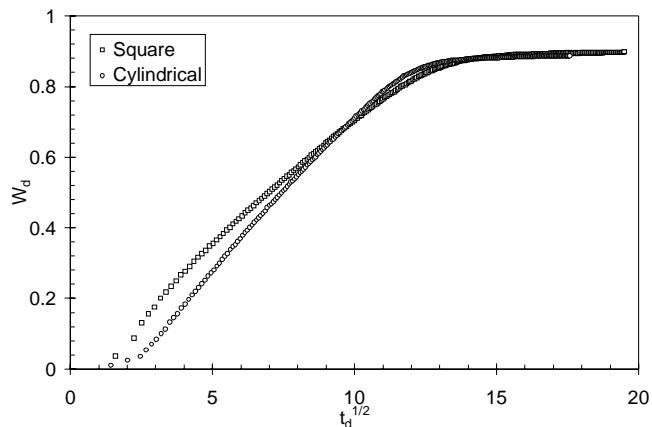


Figure 4. Spontaneous imbibition in cylindrical and square cores (Berea sandstone).

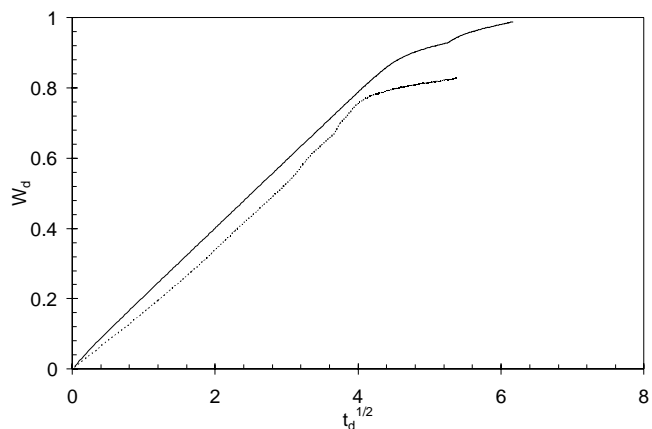


Figure 5. Spontaneous imbibition in diatomite - repeatability tests.

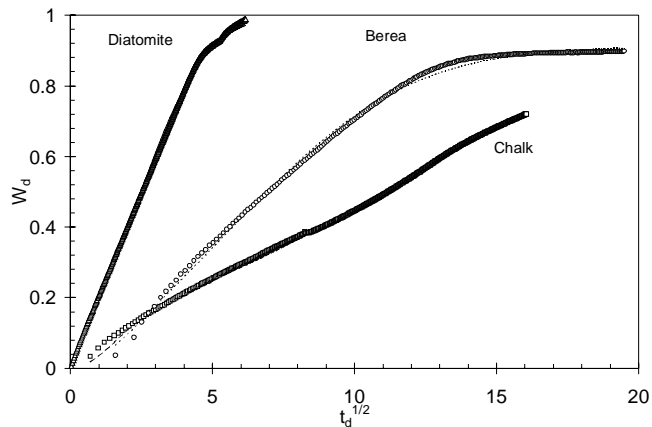


Figure 6. Spontaneous imbibition in chalk, diatomite, and Berea sandstone compared to model fit.

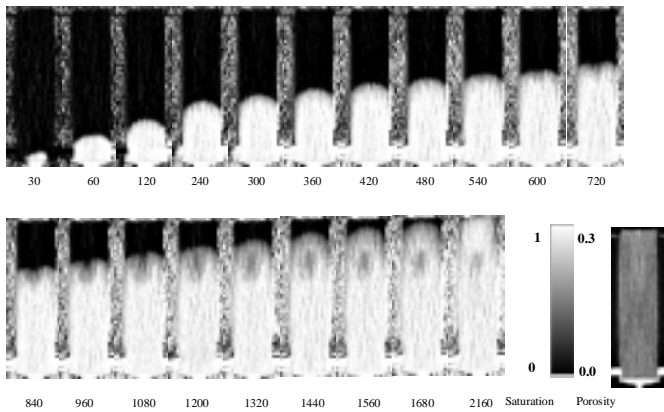


Figure 7. Water saturation images of spontaneous imbibition in Berea sandstone at different times (sec).

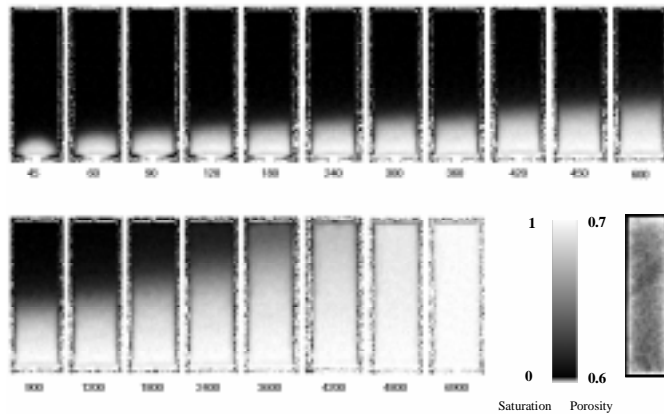


Figure 8. Water saturation images of spontaneous imbibition in diatomite at different times (sec).

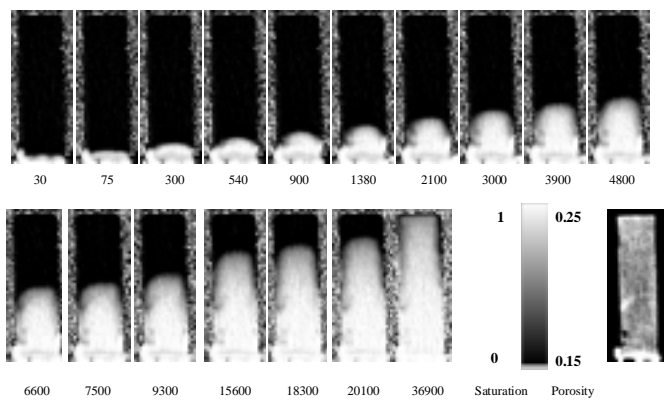


Figure 9. Water saturation images of spontaneous imbibition in chalk at different times (sec).